BIO-INSPIRED MULTIDIRECTIONAL LAMINATES FOR IMPROVED COMPRESSIVE PERFORMANCE

Torquato Garulli[1,*], Tomas J. Katafiasz[2], Emile S. Greenhalgh[3] and Silvestre T. Pinho[4]

[1] Department of Aeronautics, Imperial College London, South Kensington, London SW7 2AZ, UK, t.garulli@imperial.ac.uk. *T. Garulli is now a Marie-Curie Postdoctoral Fellow at the University of Girona (torquato.garulli@udg.edu). The work presented in this paper was carried out when he was a Postdoctoral Research Associate at Imperial College London.

[2] Department of Aeronautics, Imperial College London, South Kensington, London SW7 2AZ, UK, tomas.katafiasz11@imperial.ac.uk

[3] Department of Aeronautics, Imperial College London, South Kensington, London SW7 2AZ, UK, e.greenhalgh@imperial.ac.uk

[4] Department of Aeronautics, Imperial College London, South Kensington, London SW7 2AZ, UK, silvestre.pinho@imperial.ac.uk, https://pinholab.cc.ic.ac.uk/

Keywords: Bio-inspiration, Compression, Microstructural design

ABSTRACT

In this study, we developed a novel microstructure inspired by the deep-sea glass sponge *Monoraphis chuni* to enhance longitudinal compressive performance of multidirectional carbon fibre reinforced polymer laminates. The microstructure features alternating stiff and soft regions, similar to those observed in the sponge's anchoring spicula. To create this microstructure, we utilized a unique manufacturing process. We then assessed the performance of the microstructure through small-scale notched compression tests, comparing it to an industrially-relevant baseline laminate. Our findings demonstrated a statistically significant increase in failure load and average ligament specific stress at failure compared to the baseline, as well as the ability to delay damage initiation and arrest damage propagation. Our research provides valuable insights for the design of lightweight structures under compression.

1 INTRODUCTION

While the adoption of high-performance carbon fibre reinforced polymers (CFRPs) for lightweight structures is steadily growing, their relatively poor properties under longitudinal compression, compared to tension, represents a limitation in many applications [1]. In unidirectional (UD) CFRPs, failure under compression most often occurs through kinkband formation and propagation [2-4]. In multidirectional (MD) laminates, other mechanisms may be involved and make the failure process even more complex [5, 6]. Consequently, improving compressive performances of MD CFRPs is a tough challenge.

In view of this, taking inspiration from naturally-occurring materials and microstructures can be of great help [7, 8]. One fascinating microstructural solution observed in nature is the periodic alternation of stiff (and strong) and soft (and weak) layers, which often characterise biomaterials with excellent fracture properties, as observed in the giant anchoring spicula of the deep-sea sponge *Monorhaphis chuni*. In these microstructures, a paramount role is played by the soft layers, as they act as crack blunting regions [9], they promote crack deflection [10], and the periodic change in properties caused by their presence is at the base of the inhomogeneity effect, which is believed to contribute to crack arrest [11].

In this work, we present a bio-inspired concept for the microstructural modification of MD CFRP laminates with the goal of improving their compressive performance. A more in-depth presentation of this study is presented in [12].

2 MICROSTRUCTURE DESIGN

2.1 Concept

We consider, for this work, traditional *quad* laminates, i.e., laminates using 0°, ±45° and 90° oriented plies. We propose to modify such laminates by the introduction of a soft phase in the 0° plies, in the form of continuous strips aligned with the load direction, as shown in the schematic sketch in Fig. 1a. Our goal is to replicate, within the load-bearing layers of the laminate, the periodic alternation of stiff and soft regions observed in biologically occurring layered materials, with the following objectives (as explained in more detail in [12]):

- Exploiting the inhomogeneity effect. The inhomogeneity effect is a change in crack driving force caused by changes in stiffness and/or strength of the material through which crack propagation is taking place. In materials with periodically changing properties, this effect may promote crack arrest and renucleation at each repetitive unit of the microstructure, greatly enhancing fracture properties. The proposed microstructural modification creates in the laminate longitudinal stripe-shaped regions where 0° CFRP material is substituted by a soft/weak material (thus soft/weak regions with respect to longitudinal compressive loading), alternated with full composite regions, containing 0° CFRP material (hence much stiffer and stronger);
  Blunting kinkbands. Final compression failure of a MD laminate coincides with the loss of its load bearing capability due to failure of the 0° plies. These fail due to kinkband formation and propagation, often facilitated by delamination. Kinkband propagation occurs under the driving force of remote loading, but also of local conditions: at the tip of the kinkband, fibres bend causing increased shear stresses ahead of them; this facilitates further local deformation, softening / fracture of the resin/interface, and eventually kinkband propagation, see Fig. 1b. In the devised concept, the presence of the soft/weak phase, unable to transfer significant shear stress and physically interrupting the 0° plies, is hypothesised to mitigate this mechanism.

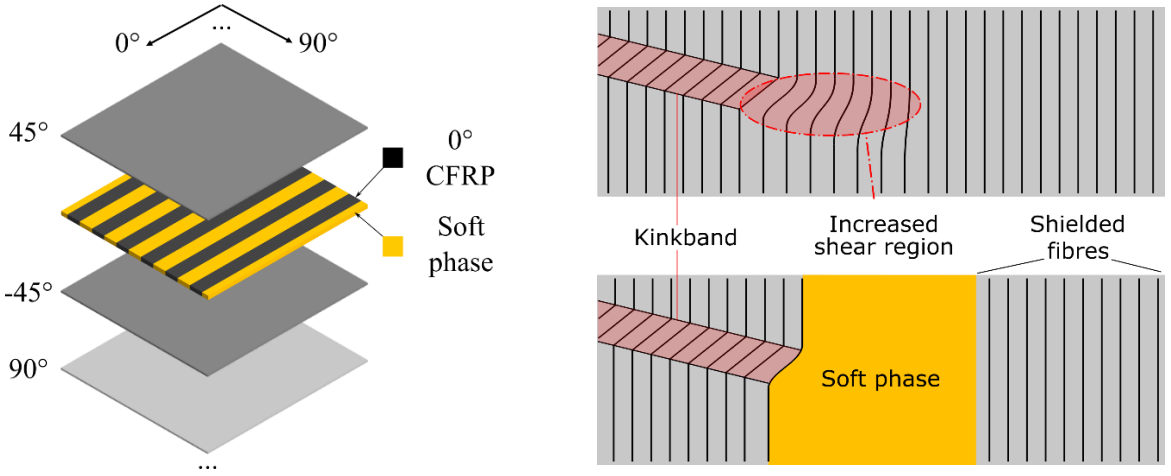

(a) (b)

Figure 1: after Garulli et al. [12], (a) schematic representation of the proposed concept: a soft/weak phase is introduced in the load bearing 0° plies of a laminate in the form of longitudinal (load aligned) strips; (b) expected beneficial effect of the presence of a soft/weak phase on the propagation of kinkbands in 0° plies.

2.2 Configuration design

For this study, we used MR70/TP402 carbon/epoxy prepreg with a Fibre Areal Weight (FAW) of 15 gsm. Properties of the constituents of the prepreg are reported in Table 1, while estimated ply properties

are reported in Table 2. As a material for the soft inclusion, we selected Rohacell RC200SL, which is a polymethacrylimide (PMI) foam material; this was kindly provided by Yoneshima Felt Ltd. in the form of 70 μm thick sheets. Properties for this material are reported in Table 3.

MR70 carbon fibre			TP402 epoxy		
*Diameter	μm	5.0	*Density	g/cm^3	1.21
*Density	g/cm^3	1.82	*Young's modulus	GPa	3.44
*Axial Young's modulus	GPa	325	†Poisson's ratio	-	0.35
†Transverse Young's modulus	GPa	25	*Tensile strength	MPa	62
†Axial shear modulus	GPa	10	Notes		
†Axial Poisson's ratio	-	0.2	* Obtained from technical datasheet		
†Transverse Poisson's ratio	-	0.22	† Assumed from experience or literature on similar materials		
*Longitudinal Tensile strength	MPa	7000			

Table 1: properties of the constituent materials of the prepreg material used, after Garulli et al. [12].

MR70/TP402 ply properties			Notes
*Density	g/cm^3	1.545	* Rule of mixtures, E_{1c} corrected to account for typical compressive/tensile moduli difference.
*Longitudinal compressive modulus, E_{1c}	GPa	153	
†Transverse moduli, E_2=E_3	GPa	9.55	† Halpin-Tsai formulas.
‡Shear moduli, G_{12}=G_{13}	GPa	4.39	‡ Cylindrical assemblage model, matrix dominated.
†Transverse shear modulus, G_{23}	GPa	3.54	
ᵗPoisson's ratios, ν_{12}=ν_{13}	-	0.26	ᵗ Periodic microstructure model.
ᵗTransverse Poisson's ratio, ν_{23}	-	0.5	
ᵛLongitudinal compressive strength, X_c	MPa	1850	ᵛ Back-calculated from in-house uniaxial compression tests on MD coupons
*Longitudinal tensile strength, X_t	MPa	3880	
▫Transverse compressive strength, Y_c	MPa	160	▫ Assumed from experience or literature on similar materials
▫Transverse tensile strength, Y_t	MPa	40	
▫In-plane shear strength, S_l	MPa	63	

Table 2: estimated properties of the prepreg material used in this study, along with information on how they have been estimated, after Garulli et al. [12].

RC200SL material properties		
Density	g/cm^3	0.205
Compressive modulus, E_c	GPa	0.37
Shear modulus, G	GPa	0.123
Compressive strength, X_c	MPa	9.6
Tensile strength, X_t	MPa	10.4
Shear strength, S_l	MPa	4.8

Table 3: Material properties of Rohacell RC200SL, as reported in the product datasheet.

As a *Baseline* configuration, we considered a standard quasi-isotropic (QI) laminate with the following layup: $[45/90/-45/0_2/45/90/-45]_{10S}$. To obtain the *Bio-inspired* (*Bio* hereafter) configuration, we doubled the number of 0° plies, but substituted half of the 0° CFRP material with the soft inclusions in the form of equally spaced, 1 mm wide, longitudinal strips, as schematically shown in Fig. 2. Thus, the overall amount of CFRP material is preserved in the *Bio* configuration, the thickness of the laminate is slightly increased, and the desired alternation of stiff/strong regions (full CFRP with a $[45/90/-45/0_4/45/90/-45]_{10S}$ layup) and soft/weak regions (CFRP and PMI foam with a $[45/90/-45/RC200SL/45/90/-45]_{10S}$ layup) is obtained.

It was reported that layered microstructures with modulus and strength ratios (properties of the soft/weak region divided by those of the stiff/strong one) equal to or lower than 0.20 and 0.30, respectively, may achieve crack arrest due to the inhomogeneity effect [13,14]. Using Classic Lamination Theory (CLT) and the LaRC05 [15] failure criterion, we estimated the equivalent longitudinal modulus and the first ply failure (FPF) strength of the two different regions of the *Bio* laminate; we then evaluated the ratios of these properties and found them to be 0.20 and 0.28, respectively; consequently, the Bio configuration devised is expected to benefit from the inhomogeneity effect.

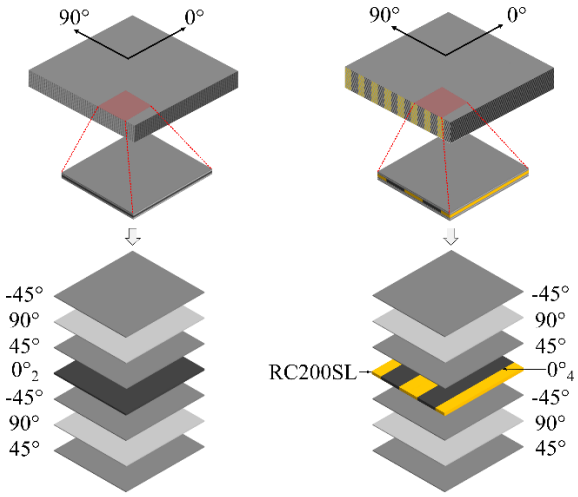

Figure 2: Schematic representation of the laminate configurations designed for this study: *Baseline* on the left and *Bio* on the right, after Garulli et al. [12].

3 MANUFACTURING AND TESTING

3.1 Manufacturing

We manufactured two plates, 100 mm wide and 75 mm long:

- *Baseline* plate: $[45/90/-45/0_2/45/90/-45]_{10S}$;
- *Bio* plate: $[45/90/-45/0_{4F}/45/90/-45]_{10S}$, where the notation 0_{4F} indicates the layers containing the foam inserts.

For the *Bio* plate we developed a bespoke manufacturing procedure, consisting in the following:

1. Material preparation: the PMI foam sheets, the prepreg and thin PET sheets (then used to create layup templates) are cut into rectangular shapes of the desired size;
2. Preliminary ply-blocks layup: partial ply blocks, i.e. $[0]_4$, [45/90/-45] and [-45/90/45] blocks, are laid up separately;

3. Laser micro-machining: the PMI sheets and the $[0]_4$ ply blocks are machined to obtain the complementary striped pattern required to create the microstructure described in Section 2. PET sheets are machined to create templates to guarantee consistent placement of the machined $[0]_4$ ply blocks during layup;
4. Complete ply-block assembling: each repetitive unit of the laminate is created by: i) laying the machined $[0]_4$ ply blocks on top of the appropriate off-axis plies block; ii) laying the machined PMI foam sheets such that the foam strips fall perfectly in between the CFRP strips; iii) completing the layup with the remaining off-axis ply block.

The plates were cured in an autoclave according to the manufacturer's recommendation, at a pressure of seven bars. More details are provided in [12].

3.2 Testing

To evaluate the performance of the novel microstructure, we tested under compression a set of small-scale notched specimens, as sketched in Fig. 3a. The specimens' faces in contact with the loading platens were ground flat and parallel. The sharp notch was created using a disk saw. From the *Bio* plate, we prepared specimens where the tip of the notch is located in a full composite region (Bio_c specimens) and specimens where the tip of the notch is located in a region containing foam strips (Bio_f specimens).

We performed the tests using a Deben micro-testing device with a 5 kN load cell, Fig. 3b. A relative compressive displacement was applied, at a rate of 0.1 mm/min, to the top and bottom faces of the specimens. For all specimen types, we performed tests using different techniques (more details provided in [12]):

- In-situ SEM tests, in which we observed damage initiation and evolution at the tip of the notch;
- Incremental tests with 2D X-ray scans, to study the progression of internal damage;
- DIC tests, to observe the evolution of the strain field during the tests.

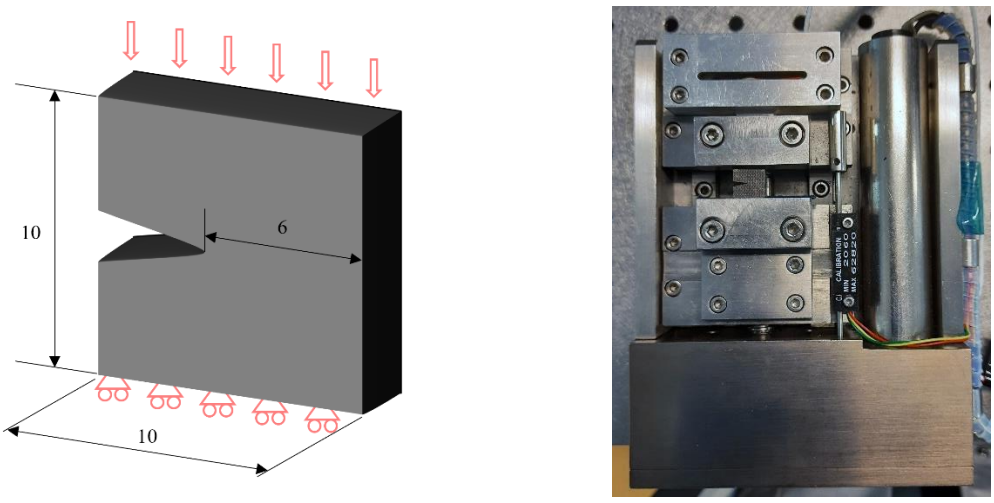

(a) (b)

Figure 3: (a) Sketch of the geometry and loading conditions of the small-scale notched specimens used in this study (dimensions in mm), after Garulli et al. [12]; (b) sample picture of one of the specimens loaded in the micromechanical rig.

4 RESULTS

The results presented here represent an excerpt from a more extensive set of results presented in Garulli et al. [12]. Fig. 4a shows the force-displacement curves obtained from all the specimens tested; we color-grouped the curves based on the specimen type and shifted the curves from the Bio_c and Bio_f specimens along the displacement axis by 0.1 and 0.2 mm, respectively, for clarity. It is worth noting

that two *Bio$_c$* specimens did not fail by the time the load reached 4800 N and the test had to be stopped to prevent damage to the load cell; this is indicated in Fig. 4a by upward pointing arrows.

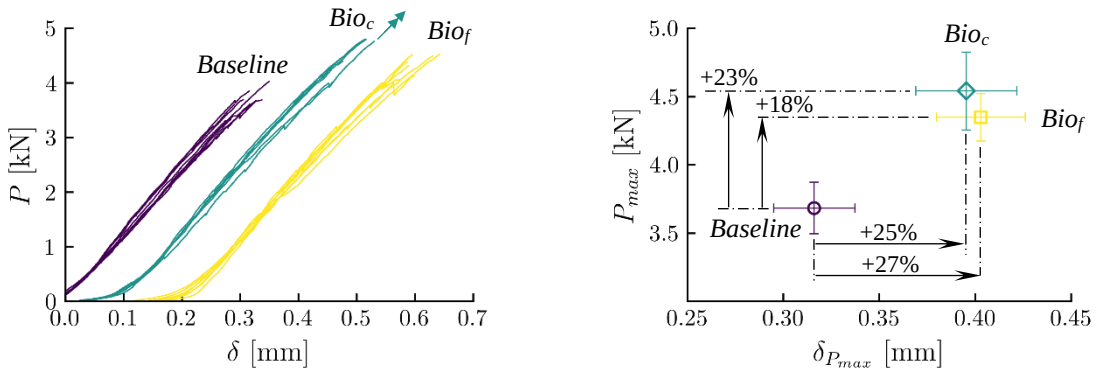

(a) (b)

Figure 4: after Garulli et al. [12], (a) Load displacement curves obtained from all specimens tested; for better visualization, the curves from *Bio$_c$* and *Bio$_f$* specimens have been translated by 0.1 and 0.2 mm, respectively, on the displacement axis; (b) average failure load and corresponding displacement for the different specimen types; error bars represent a ±1 standard deviation interval.

Fig. 4b reports the average values of failure load (P_{max}) versus failure displacement (δ_{Pmax}) for the different specimen types, along with error bars indicating a ±1 standard deviation interval; furthermore, percentage increase in failure load and failure displacement of the *Bio* specimens with respect to the *Baseline* ones are reported. To evaluate the statistical significance of these improvements, we used T-test. All the *p*-values we obtained were significantly smaller than 0.05 (commonly assumed threshold), confirming the statistical significance of the results.

Table 4 additionally reports the average values of the force per unit ligament length (l = ligament length), $\frac{P_{max}}{l}$, and the ligament specific stress at failure (t = specimen thickness, ρ = density), $\frac{P_{max}}{lt\rho}$. As shown in Table 4, the novel microstructural design not only led to an increase of the failure load, but also to an increase of the average ligament specific stress at failure.

	P_{max} (N)	$\frac{P_{max}}{l}$ (MPa mm)	$\frac{P_{max}}{lt\rho}$ (MPa cm^3 g^{-1})
Baseline	3685	627	170
Bio$_c$	≥4542	≥807	≥198
Bio$_f$	4350	729	180

Table 4: average experimental values obtained for the failure load, the failure load per ligament length and the ligament specific stress at failure, for the three different specimen types tested, after Garulli et al. [12].

Fig. 5 shows, for one specimen of each type, SEM pictures of the entire specimen and a detail of the notch tip region before loading and at an advanced stage of the test, i.e. when load reached 3200 N. Different behaviours are seen from different specimen types: damage and material crushing is evident

at 3200 N for the *Baseline* specimen and even more for the *Bio$_c$* one; on the other hand, damage is still minimal for the *Bio$_f$* specimen.

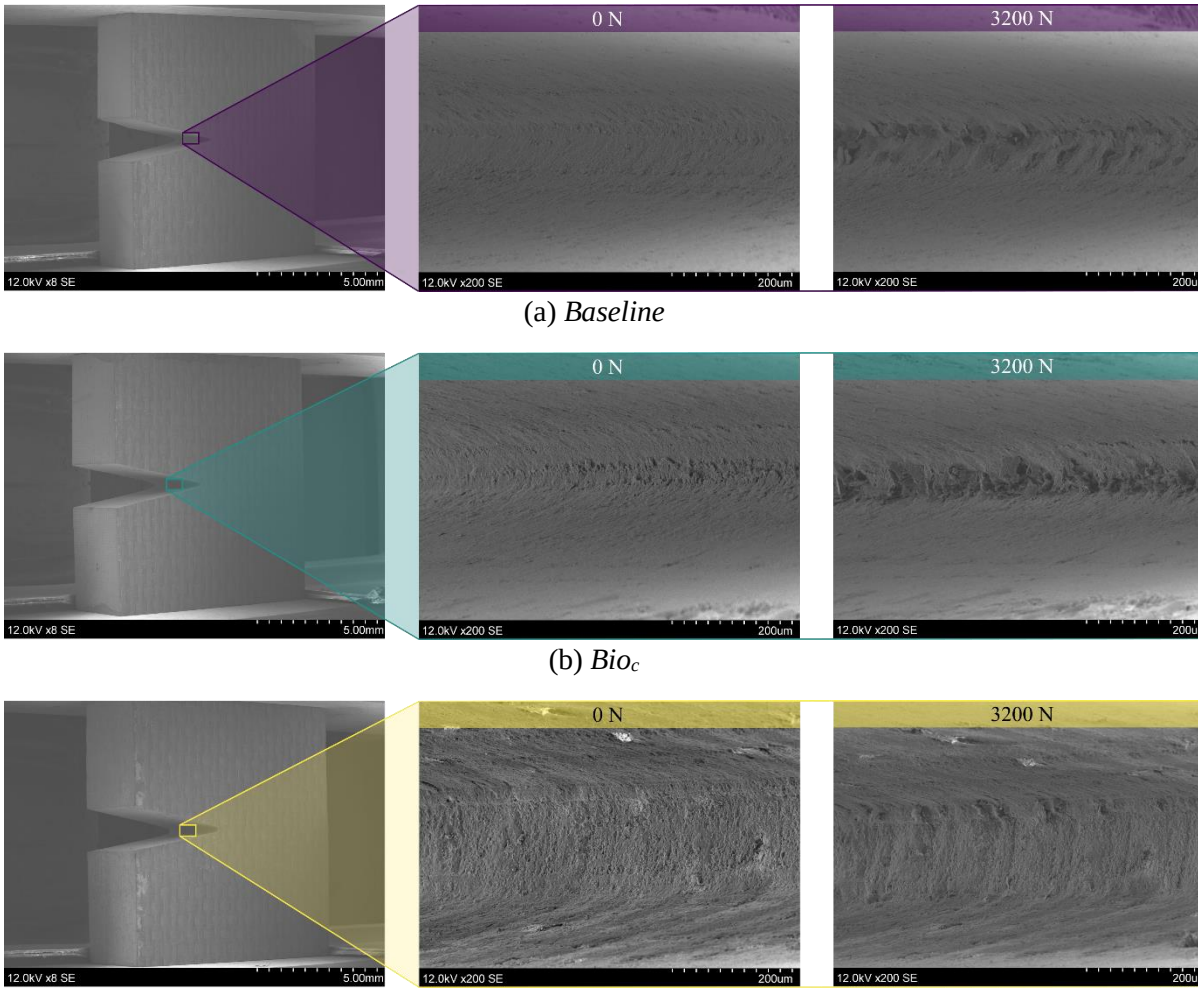

(a) *Baseline*

(b) *Bio$_c$*

(c) *Bio$_f$*

Figure 5: SEM images taken at different levels during testing of specimens of each type, after Garulli et al. [12]: (a) *Baseline*, (b) *Bio$_c$*, and (c) *Bio$_f$*.

Fig. 6 shows 2D X-ray scans after loading at different levels for one sample specimen of each type. In the scans from the *Baseline* specimen, damage propagating from the notch is clearly visible before failure, Fig. 6a. This is the case also for the *Bio$_c$* specimen, for which at 2800 N damage clearly extends through the entire stiff region and reaches the boundary with the neighboring soft region, Fig. 6b. Interestingly, after loading to 4000 N, damage appears more significant, but it seems to almost have not propagated further. From the X-ray scans of the *Bio$_f$* specimen, no damage progression from the notch tip is observed at all.

Fig. 7 shows full field contour plots of the longitudinal strain, for different load levels and for all specimen type, as obtained by DIC; the *Bio$_c$* specimen shown in Fig. 6b is one of the two that did not fail by the time the test had to be stopped.

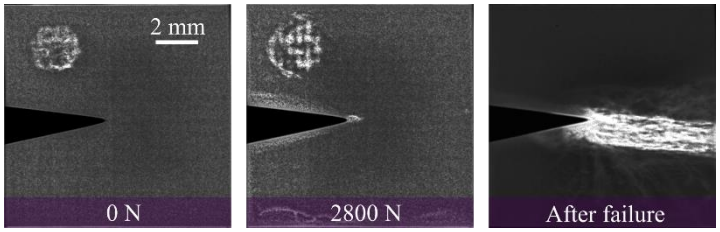

(a)

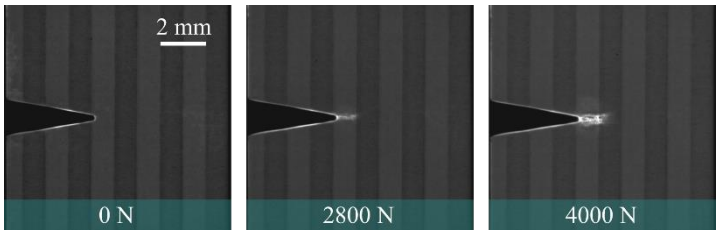

(b) *Bio$_c$*

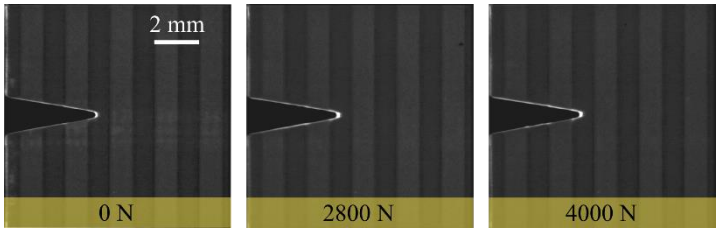

(c) *Bio$_f$*

Figure 6: 2D X-ray scans obtained after loading at different levels for one sample specimen of each type, after Garulli et al. [12]: (a) *Baseline*, (b) *Bio$_c$*, and (c) *Bio$_f$*.

5 DISCUSSION

The results presented in the previous section proved that the novel microstructure could enhance the load bearing capabilities under compression of the laminate. Moreover, the increase in failure load was larger than increase in weight (around 10%) due to the introduction of the foam material, thus resulting in an improvement of specific properties, as seen in Table 4. This improvement most likely is to be attributed to the way the novel microstructure changed the failure process under compression of the specimens. In *Baseline* specimens, during in-situ SEM tests, we observed early initiation of damage at the notch tip, at a load of about 1600 N; subsequently material crushing at the notch tip became more severe, as observed in Fig. 5a. In agreement with this, 2D X-ray scans showed damage initiating early at the notch and then propagating inside the specimen, as seen in Fig. 6a, up to a length of around 1 mm, after which the specimen would fail. Interestingly, the 2D X-ray scans do not show ply splits at ±45°, suggesting the observed damage is likely in-plane kinking in 0° plies. This may be justified by the use of an ultra-thin prepreg material, thus resulting in significant in-situ effect and hence high strength.

Bio$_c$ specimens had a similar initial behavior, including early initiation and visible propagation of damage from the notch. As seen in Fig. 6b, after loading to 2800 N, damage has propagated through the entire stiff region and reached the boundary with the next soft region. In this case too, no ±45° ply splits are visible. After subsequent loading up to 4000 N, we can observe that damage has almost not extended in the ligament direction, Fig. 6b; it thus seems that the soft region is acting as a barrier to damage propagation. Concurrently, a local intensification of damage is clearly observed: the damage area is brighter and more extended in the loading direction, suggesting more material has been involved in the damage process; also, a barely visible halo surrounds the damage area, suggesting delamination has occurred too. Despite this, the *Bio$_c$* specimens all failed at loads much higher than those of the *Baseline* ones. The longitudinal strain field obtained by DIC at peak load, Fig. 7a and 7b, show how significant

the difference is between *Baseline* and *Bio$_c$* specimens: the latter are able to withstand a much higher load even in the presence of an extremely extended area of high strain and damage.

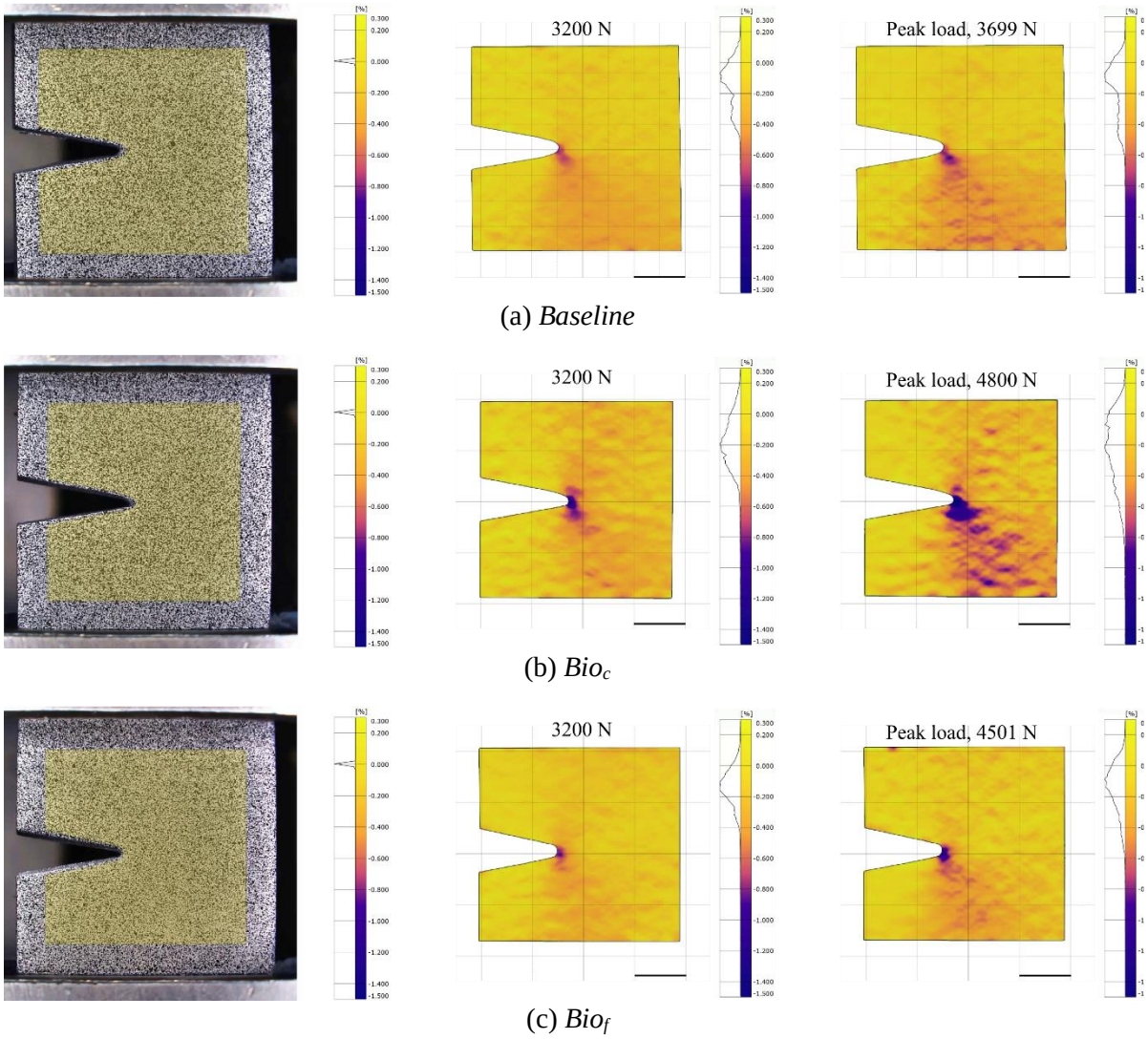

Figure 7: SEM images taken at different levels during testing of specimens of each type, after Garulli et al. [12]: (a) *Baseline*, (b) *Bio$_c$*, and (c) *Bio$_f$*.

Interestingly, *Bio$_f$* specimens showed a behavior quite different from the others. SEM images taken during the tests, Fig. 5c, showed minimal damage throughout the entire test, up to final failure. Accordingly, no damage was observed with 2D X-ray scans, Fig. 6c. It therefore seems that damage initiation was largely delayed or completely inhibited when the notch tip was located in a soft region. These regions could easily go to much larger strains than the stiffer ones without suffering failure; this suggests they may be able to blunt the notch and shield the next stiff region, leading, once again, to a failure load much higher than for the *Baseline* specimens.

6 CONCLUSIONS

In this work, we investigated a new microstructural concept to enhance in-plane compressive performance of multidirectional carbon fibre reinforced polymers laminates. The concept was inspired by the layered structure of biological materials, such as the anchoring spicula of the deep-sea glass

sponge *Monoraphis chuni*, which exhibit exceptional fracture properties.

The novel microstructure involves an in-plane alternation of stiff and soft regions, achieved by incorporating polymethacrylimide foam strips in the load bearing 0° plies. To ensure consistent results, we developed a bespoke manufacturing process that utilizes precision laser micro-machining and alignment strategies. We then evaluated the performance of the novel concept by conducting compression tests on small-scale notched specimens, with a comparable traditional quasi-isotropic laminate used as a baseline for comparison.

The novel microstructure led to 18% to 23% higher failure load when compared to the baseline, depending on the initial location of the notch tip in the specimens. Moreover, the ligament section specific stress at failure was increased too. Additionally, the novel microstructure exhibited a tendency to delay damage initiation from the notch and arrest its propagation when a soft region was reached.

The bio-inspired concept presented shows the potential to improve performance of multidirectional carbon fibre reinforced polymers laminates under compression and could therefore have a major impact on the design of lightweight structures. Future research should involve testing at coupon scale, to quantitatively assess the benefits of the concept on apparent compressive fracture toughness. Also, techniques for faster, large-scale manufacturing are required to make the concept viable for practical applications.

ACKNOWLEDGEMENTS

The authors acknowledge the funding for this research provided by UK Engineering and Physical Sciences Research Council (EPSRC) programme Grant EP/T011653/1, Next Generation Fibre-Reinforced Composites: a Full Scale Redesign for Compression in collaboration with University of Bristol. Yoneshima Felt Co. Ltd. and Tomoya Yoneshima are acknowledged for kindly providing the polymethacrylimide foam sheets used for this research.

REFERENCES

[1] S. Nunna, A. R. Ravindran, J. Mroszczok, C. Creighton and R. J. Varley, A review of the structural factors which control compression in carbon fibres and their composites, *Composite Structures*, **303**, 2023, pp. 116293 (doi: 10.1016/j.compstruct.2022.116293).

[2] S. Pimenta, R. Gutkin, S.T. Pinho and P. Robinson, A micromechanical model for kink-band formation: Part I — Experimental study and numerical modelling, *Composites Science and Technology*, **69** (7–8), 2009, pp. 948-955 (doi: 10.1016/j.compscitech.2009.02.010).

[3] S. Pimenta, R. Gutkin, S.T. Pinho and P. Robinson, A micromechanical model for kink-band formation: Part II—Analytical modelling, *Composites Science and Technology*, **69** (7–8), 2009, pp. 956-964, (doi: 10.1016/j.compscitech.2009.02.003).

[4] S.T. Pinho, R. Gutkin, S. Pimenta, N.V. De Carvalho and P. Robinson, On longitudinal compressive failure of carbon-fibre-reinforced polymer: from unidirectional to woven, and from virgin to recycled, *Philosophical Transactions of the Royal Society A: Mathematical, Physical and Engineering Sciences*, **1895**, 2012, pp. 3701871 (doi: 10.1098/rsta.2011.0429).

[5] S.A. Tsampas, E.S. Greenhalgh, J. Ankersen and P.T. Curtis, On compressive failure of multidirectional fibre-reinforced composites: A fractographic study. *Composites Part A: Applied Science and Manufacturing*, **43**, 2012, pp. 454-468 (doi: 10.1016/j.compositesa.2011.11.013)

[6] S.A. Tsampas, E.S. Greenhalgh, J. Ankersen and P.T. Curtis, Compressive failure of hybrid multidirectional fibre-reinforced composites, *Composites Part A: Applied Science and Manufacturing*, **71**, 2015, pp. 40-58 (doi: 10.1016/j.compositesa.2015.01.002).

[7] J. Plocher, L. Mencattelli, F. Narducci and S.T. Pinho, Learning from nature: Bio-inspiration for damage-tolerant high-performance fibre-reinforced composites, *Composites Science and Technology*, **208**, 2021, pp. 108669 (doi: 10.1016/j.compscitech.2021.108669).

[8] T. Garulli, E.S. Greenhalgh and S.T. Pinho, A novel bio-inspired microstructure for progressive compressive failure in multidirectional composite laminates, *Proceedings of the 20th European*

Conference on Composite Materials Composites Meet Sustainability (Eds. A. Vassilopoulos, V. Michaud), Lausanne, Switzerland, June 26-30, 2022, EPFL Lausanne, Composite Construction Laboratory, Vol. 1, 2022, pp. 7-13.

[9] J.C. Weaver, G.W. Milliron, P. Allen, A. Miserez, A. Rawal, J. Garay, P.J. Thurner, J. Seto, B. Mayzel, L.J. Friesen, B.F. Chmelka, P. Fratzl, J. Aizenberg, Y. Dauphin, D. Kisailus and D.E. Morse, Unifying design strategies in demosponge and hexactinellid skeletal systems, *The Journal of Adhesion*, **86** (1), 2010, pp. 72–95 (doi: 10.1080/00218460903417917).

[10] A. Miserez, J.C. Weaver, P.J. Thurner, J. Aizenberg, Y. Dauphin, P. Fratzl, D.E. Morse and F.W. Zok, Effects of laminate architecture on fracture resistance of sponge biosilica: Lessons from nature, *Advanced Functional Materials*, **18** (8), 2008, pp. 1241–1248 (doi: 10.1002/adfm.200701135).

[11] O. Kolednik, J. Predan, F. Fischer and P. Fratzl, Improvements of strength and fracture resistance by spatial material property variations, *Acta Materialia*, **68**, 2014, pp. 279–294 (doi: 10.1016/j.actamat.2014.01.034).

[12] T. Garulli, T.J. Katafiasz, E.S. Greenhalgh and S.T. Pinho, A novel bio-inspired microstructure for improved compressive performance of multidirectional CFRP laminates. *Composites Part B: Engineering*, paper submitted.

[13] P. Fratzl, H. Gupta, F. Fischer and O. Kolednik, Hindered crack propagation in materials with periodically varying young's modulus—lessons from biological materials, *Advanced Materials*, **19** (18), 2007, pp. 2657–2661 (doi: 10.1002/adma.200602394.570).

[14] J. Wiener, F. Arbeiter, O. Kolednik and G. Pinter, Influence of layer architecture on fracture toughness and specimen stiffness in polymer multilayer composites, *Materials & Design*, **219**, 2022, pp. 110828 (doi: 10.1016/j.matdes.2022.110828.545).

[15] S. Pinho, R. Darvizeh, P. Robinson, C. Schuecker and P. Camanho, Material and structural response of polymer-matrix fibre-reinforced composites, *Journal of Composite Materials*, **46** (19-20), 2012, pp. 2313–2341 (doi: 10.1177/0021998312454478).